Supplementary Information for

Visible-light excitable, highly transparent and luminescent films consisted of ultrahighly loaded europium(III) complex

Yuan Wang[a], Guangmin Xie[a], Jinglei Chen[a], Xiurong Zhang[b], Cong Chen, Jian Yin[b]* and Huanrong Li[a]*

[a]Tianjin Key Laboratory of Chemical Process Safety, School of Chemical Engineering and Technology, Hebei University of Technology, Guangrong Dao 8, Hongqiao District, Tianjin, 300130, PR China
[b]Tianjin Baogang Research Institute of Rare Earths Co., Ltd., Tianjin 300300, China

Corresponding Author

Jian Yin: yinjian425@sina.com

Huanrong Li: lihuanrong@hebut.edu.cn

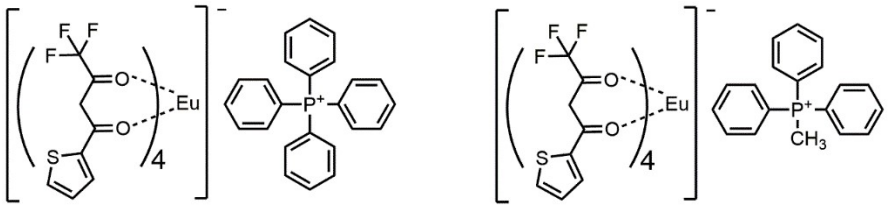

Scheme S1. general formula of complexes **1** and **2**.

Complex **1**. FT-IR: 1610 cm^{-1}, 1535 cm^{-1} ($\nu_{C=O}$), 1471 cm^{-1} ($\nu_{C=C}$, benzene ring), 1184 cm^{-1} (ν_{C-P}), 1137 cm^{-1} (ν_{C-F}), 580 cm^{-1} ($\nu_{C=S}$, thiophene ring); ^1H NMR (400 MHz, $CDCl_3$, δ): 9.26-9.16 (d, 16H), 8.79 (s, 1H), 6.87-6.79 (d, 8H), 6.58 (s, 4H), 4.03 (s, 1H). Anal. calcd: C 48.69, H 2.61; found: C 47.90, H 2.13.

Complex **2**. FT-IR: 1608 cm^{-1}, 1535 cm^{-1} ($\nu_{C=O}$), 1473 cm^{-1} ($\nu_{C=C}$, benzene ring), 1184 cm^{-1} (ν_{C-P}), 1139 cm^{-1} (ν_{C-F}), 578 cm^{-1} ($\nu_{C=S}$, thiophene ring); ^1H NMR (400 MHz, $CDCl_3$, δ): 10.36 (m, 6H), 8.65-8.49 (m, 9H), 7.08 (d, 4H), 6.87 (s, 4H), 6.67 (s, 4H), 4.80 (s, 3H), 3.56 (s, 4H). Anal. calcd: C 46.43, H 2.58; found: C 45.89, H 2.12.

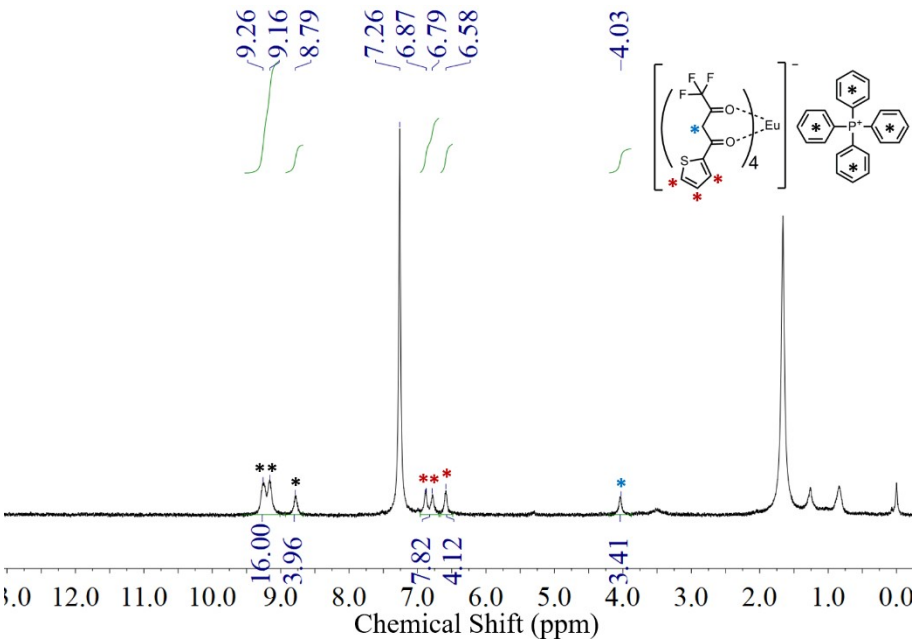

Figure S1. ^1H NMR spectrum of complex **1** ($CDCl_3$, 400 MHz, 25 °C).

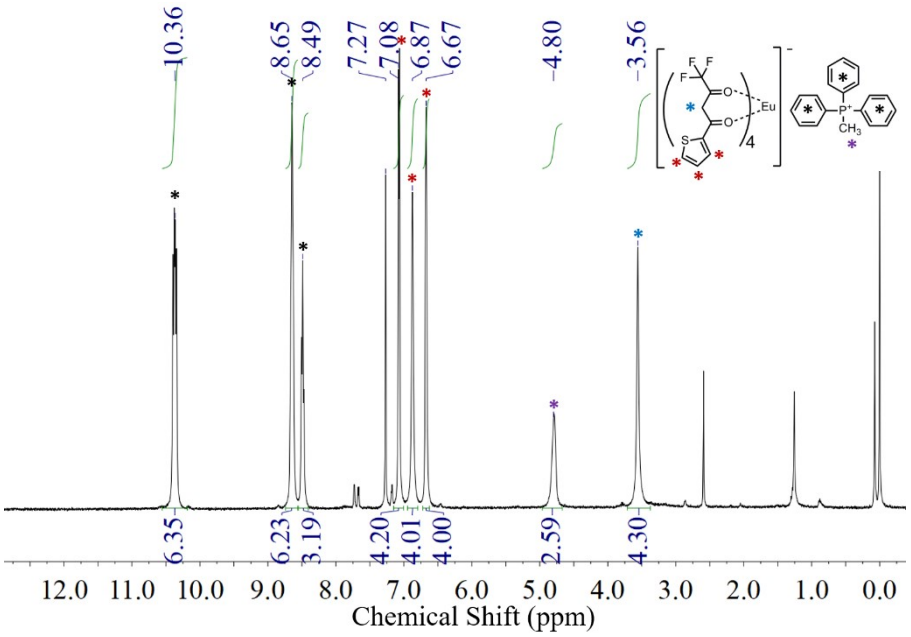

Figure S2. ^{1}H NMR spectrum of complex **2** ($CDCl_3$, 400 MHz, 25 °C).

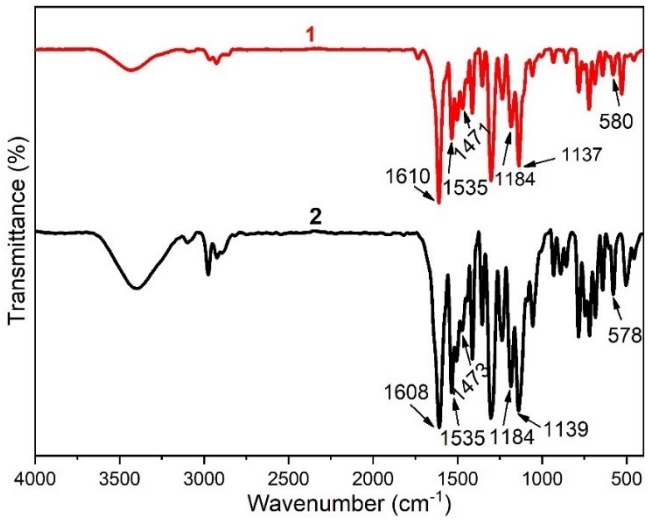

Figure S3. FT-IR spectra of complexes **1** and **2**.

Table S1. Single crystal data of complex **1**.

Empirical formula	$C_{56}H_{36}EuF_{12}O_8PS_4$
Formula weight	1376.02
Temperature/K	109 (15)
Crystal system	triclinic
Space group	$P\bar{1}$
a/Å	12.5388 (5)
b/Å	14.6688 (6)
c/Å	16.2920 (7)
α/°	84.687 (3)
β/°	83.102 (3)
γ/°	77.416 (3)
Volume/Å^3	2896.6 (2)
Z	2
ρ_{calc}g/cm^3	1.578
μ/mm^{-1}	10.165
F (000)	1372.0
Crystal size/mm^3	0.12 × 0.11 × 0.1
Radiation	Cu Kα (λ = 1.54184)
2Θ range for data collection/°	7.98 to 152.3
Index ranges	-15 ≤ h ≤ 14, -14 ≤ k ≤ 18, -20 ≤ l ≤ 19
Reflections collected	28843
Independent reflections	11 592 [R_{int} = 0.0741, R_{sigma} = 0.0672]
Data/restraints/parameters	11592/795/904
Goodness-of-fit on F^2	1.047
Final R indexes [I>=2σ (I)]	R_1 = 0.0903, wR_2 = 0.2405
Final R indexes [all data]	R_1 = 0.1013, wR_2 = 0.2469
Largest diff. peak/hole / e Å^{-3}	3.11/-2.16
CCDC	2087952

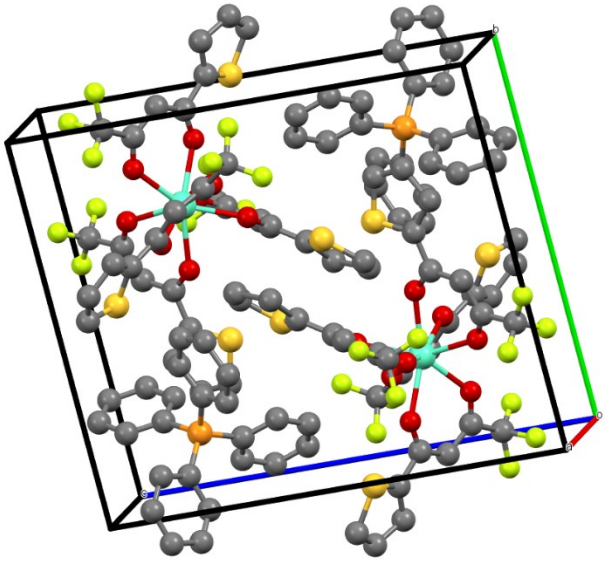

Figure S4. The view of the crystal packing of complex **1**.

Table S2. Selected bond lengths (Å) and angles (°) for complex **1**.

Eu1-O13	2.361(5)	Eu1-O16	2.358(6)
Eu1-O14	2.409(6)	Eu1-O17	2.379(6)
Eu1-O15	2.402(6)	Eu1-O18	2.389(5)
Eu1-O19	2.395(6)	Eu1-O20	2.381(6)
O13-Eu1-O14	71.54(19)	O13-Eu1-O15	75.5(2)
O13-Eu1-O17	71.70(19)	O13-Eu1-O18	89.55(19)
O13-Eu1-O19	137.4(2)	O13-Eu1-O20	149.1(2)
O15-Eu1-O14	135.14(19)	O16-Eu1-O13	106.1(2)
O16-Eu1-O14	72.53(19)	O16-Eu1-O15	147.3(2)
O16-Eu1-O17	72.98(19)	O16-Eu1-O18	134.64(19)
O16-Eu1-O19	89.9(2)	O16-Eu1-O20	72.3(2)
O17-Eu1-O14	118.8(2)	O17-Eu1-O15	76.9(2)
O17-Eu1-O18	151.22(19)	O17-Eu1-O19	76.1(2)
O17-Eu1-O20	132.99(19)	O18-Eu1-O14	72.80(19)
O18-Eu1-O15	77.4(2)	O18-Eu1-O19	107.0(2)
O19-Eu1-O14	150.5(2)	O19-Eu1-O15	70.6(2)
O20-Eu1-O14	78.8(2)	O20-Eu1-O15	123.0(2)
O20-Eu1-O18	73.0(2)	O20-Eu1-O19	73.2(2)

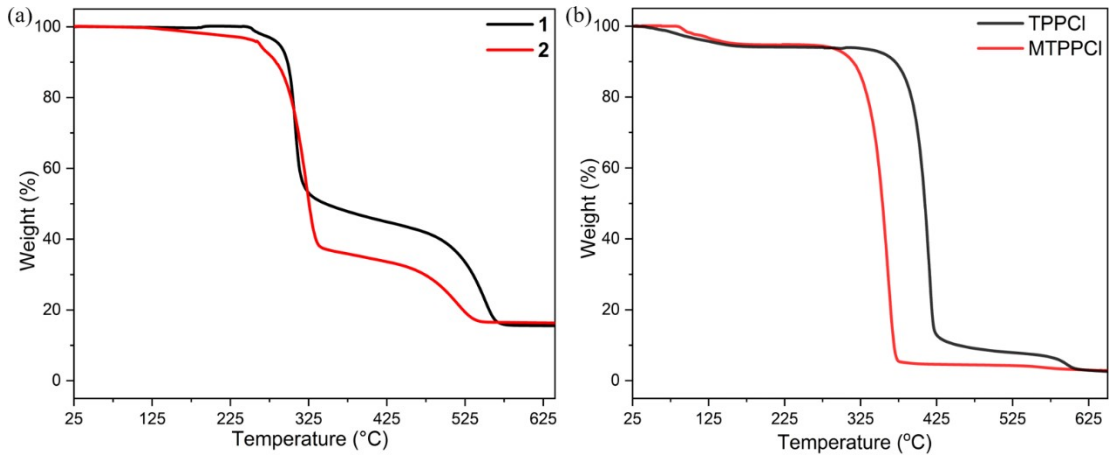

Figure S5. Thermal gravimetric analysis curves of the (a) complexes **1** and **2** and (b) TPPCl and MTPPCl.

The thermal stability of complexes **1** and **2** was performed in Figure S5a. It can be found that they exhibit the similar destruction trends. Take complex **1** as an example, there is no significant weight loss within the temperature range of 25-250 ºC, indicating that the absence of H_2O and solvent molecules in the complex. Further heating above 250 ºC leads to the decomposition of the complex. The decomposition consists of three weight losses in the steps around 250-335, 335-480 and 480-570 °C. Due to the main thermal decomposition observed to be >350 ºC for TPPCl (Figure S5b), it is speculated that the first stage can be signed to the loss of TTA and another two step one corresponds to the loss of the mixture of TTA and TPP^+, respectively.

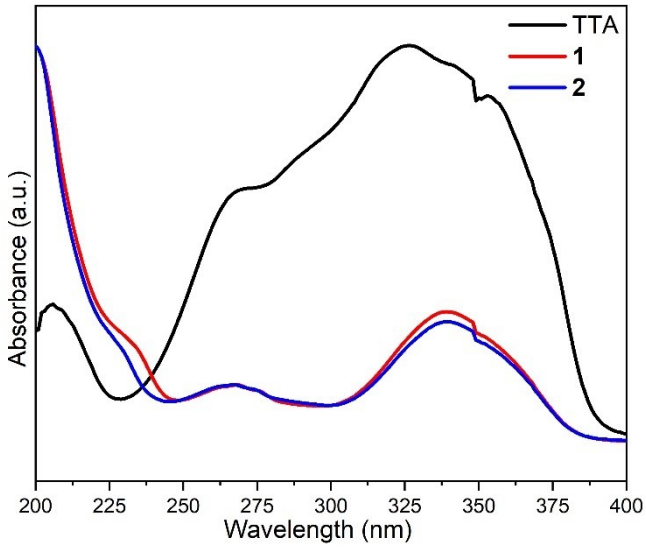

Figure S6. UV-vis absorption spectra of the ligand TTA and the complexes **1** and **2** in ethanol solution at room temperature.

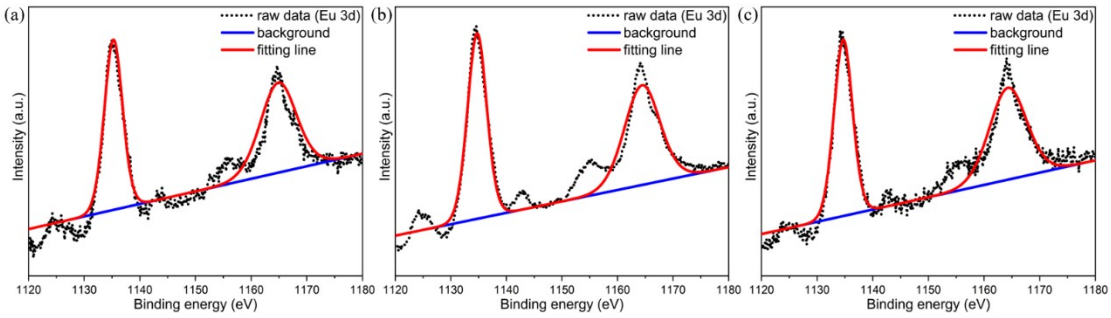

Figure S7. High-resolution XPS fitting result for the Eu 3d spectrum of complexes **1** (a), **2** (b) and **3** (c).

Table S3. Binding energy values of O 1s and Eu 3d.

Complexes	Eu 3d (eV)
1	1 134.71/1 164.30
2	1 134.73/1 164.43
3	1 135.25/1 164.89

Calculation of nonradiative rate constant k_{nr} and radiative rate constant k_r:

$$K_{nr} = \frac{1}{\tau_{obs}} - \frac{1}{\tau_{rad}} \quad \text{(eq S1)}$$

$$K_r = \frac{1}{\tau_{rad}} = A_{MD,0} \bullet n^3 \bullet \left(\frac{I_{tot}}{I_{MD}} \right) \quad \text{(eq S2)}$$

Where τ_{obs} is the observed emission lifetime determined by experiment. τ_{rad} is the radiative lifetimes of Eu^{3+}, being obtained from equations S2. A_{MD} is the spontaneous emission probability of the $^5D_0 \rightarrow {}^7F_1$ transition being 14.65 s^{-1} in vacuo and n means the refractive index of the medium that is equal to 1.5 in the calculation. I_{tot}/I_{MD} signifies the ratio of the integrated emission spectrum and the integrated intensity of the $^5D_0 \rightarrow {}^7F_1$ transition.

Table S4. Photophysical data for the complexes **1**, **2** and **3**.

Complexes	I_{tot}/I_{MD}	τ_{obs} (ms)	τ_{rad} (ms)	K_r (s^{-1})	K_{nr} (s^{-1})	Φ_{tot} (%)
1	20.91	0.436	0.967	1033.87	1 259.45	59.72
2	18.41	0.418	1.099	910.25	1 482.42	61.05

3	16.63	0.222	1.216	822.27	3 701.94	21.58

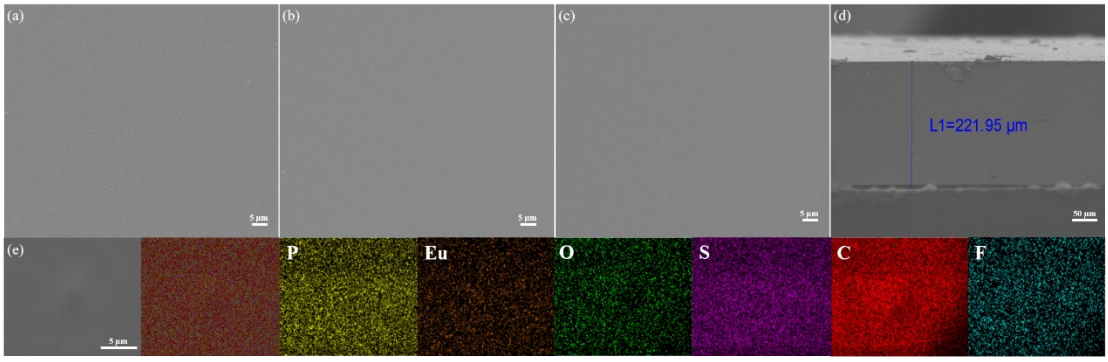

Figure S8. (a-c) SEM surface morphology of the luminescent films containing 5 wt %, 50 wt % and 80 wt % loading contents of complex **1**. (d) Cross-sectional morphology and (e) EDX mapping of the luminescent film with 80 wt % loading content of complex **1**.

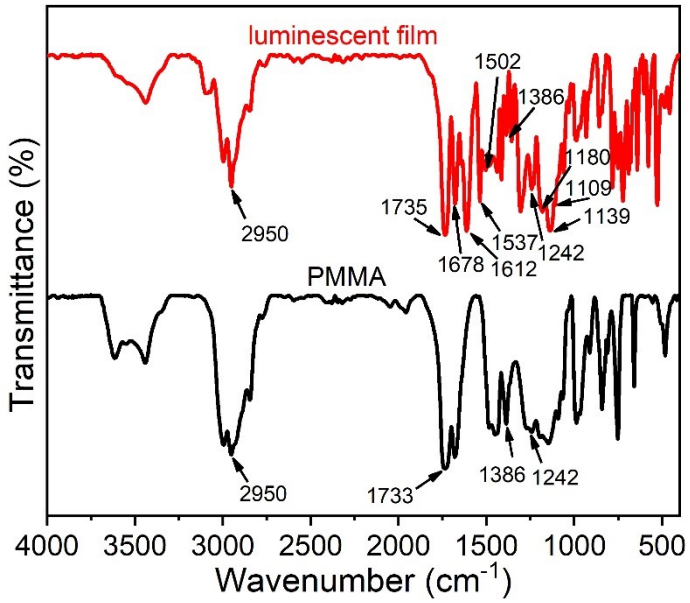

Figure S9. FT-IR spectra of PMMA and luminescent film with 50 wt % loading content of complex **1**.

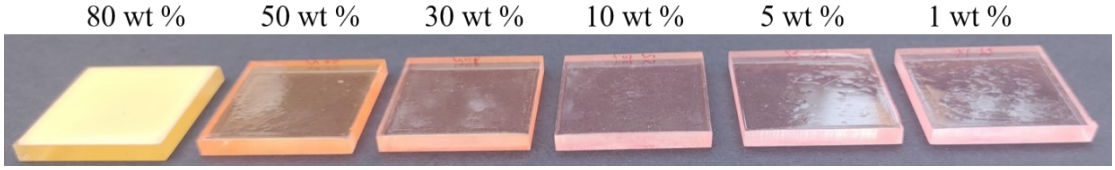

Figure S10. Digital photographs of the luminescent film with different contents of complex **3** under day light.

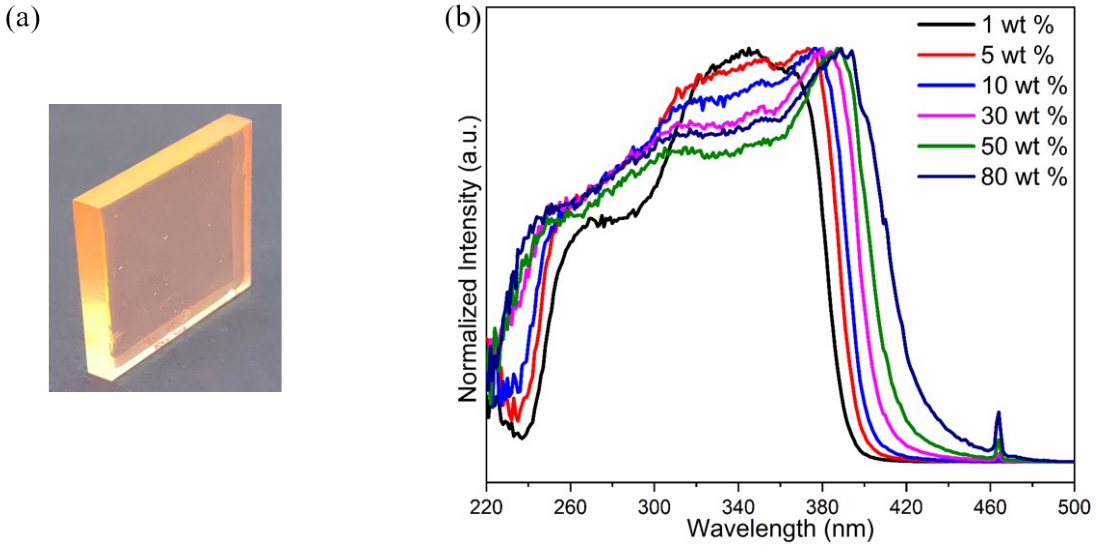

Figure S11. (a) Digital photographs of the luminescent film with complex **2** loading content of 80 wt %; (b) Excitation spectra of the luminescent films with different contents of complex **2**.

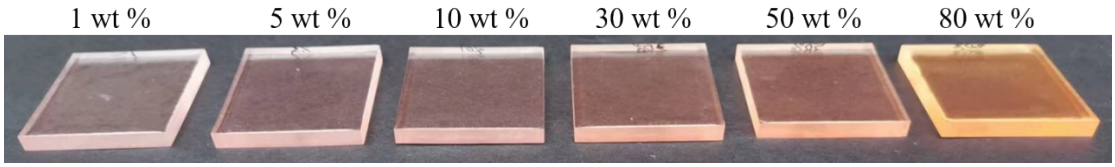

Figure S12. Digital photographs of the luminescent film with different contents of complex **1** under day light.

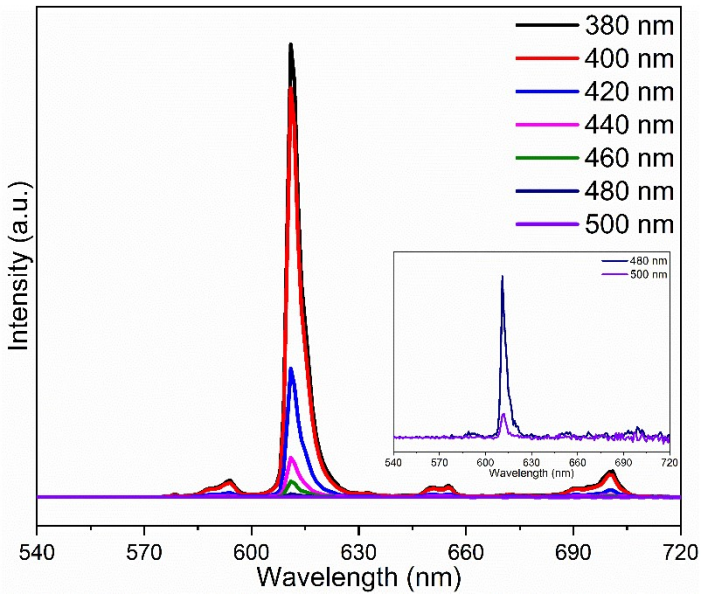

Figure S13. The emission spectra of the luminescent films with 80 wt % content of the complex **1** under the different excitation wavelength.

Table S5. Photophysical data for the luminescent films with different content of complex **1**.

	1 wt %	5 wt %	10 wt %	30 wt %	50 wt %	80 wt %
τ_{obs} (ms)	0.49	0.47	0.48	0.49	0.47	0.43
Φ_{tot} (%)	65.44%	61.67%	66.92%	60.03%	64.92%	62.52%

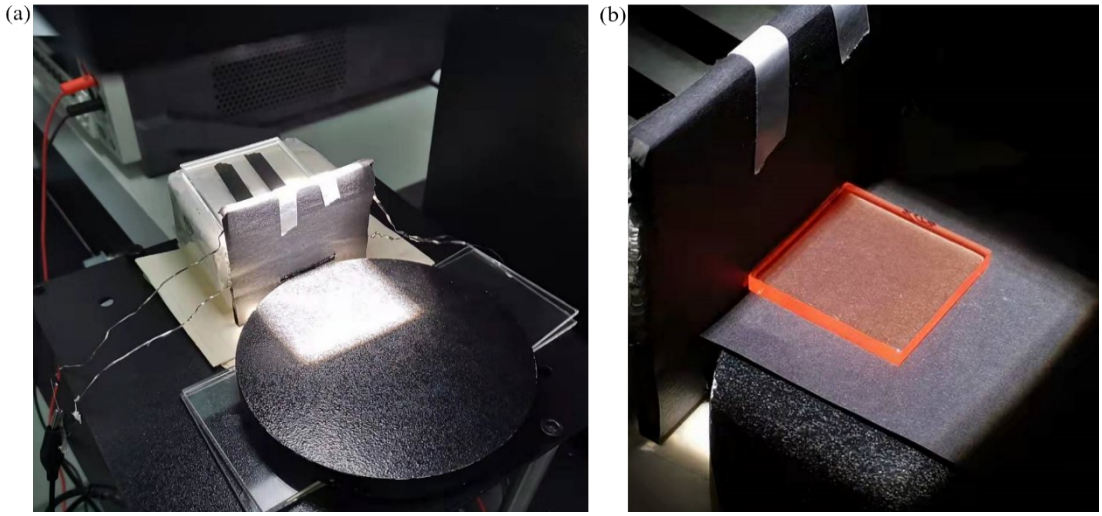

Figure S14. Schematic diagrams of the setup in measuring the *J*-*V* performance of the LSC.

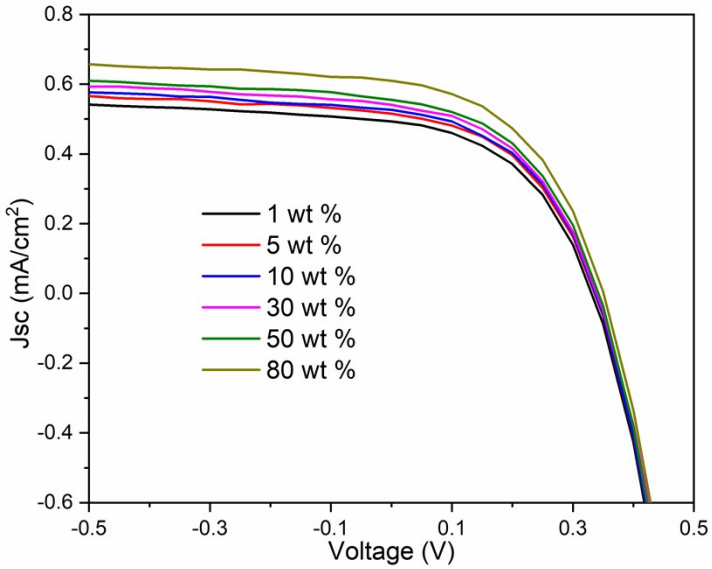

Figure S15. *J-V* curves of the LSC with different contents of complex **1**.

Table S6. Performance parameters of the LSC with different contents of complex **1**.

LSC	V_{OC} (V)	J_{SC} (mA/cm^2)	FF (%)	P_{out} (mW)	PCE (%)	η_{opt} (%)
0 wt %	0.30	0.44	49.05	0.59	0.065	3.94
1 wt %	0.30	0.49	50.20	0.67	0.074	4.37
5 wt %	0.30	0.52	51.24	0.71	0.079	4.57
10 wt %	0.30	0.53	50.98	0.72	0.081	4.67
30 wt %	0.30	0.54	51.29	0.75	0.083	4.79
50 wt %	0.30	0.55	51.71	0.77	0.086	4.92
80 wt %	0.30	0.61	44.83	0.86	0.096	5.40

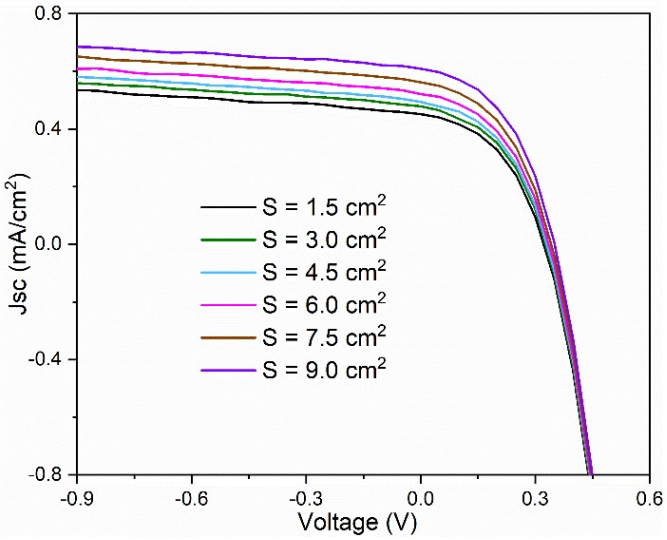

Figure S16. *J-V* curves of the LSC (80 wt % loading content of complex **1**) with different illuminated areas.